

Generation of High-Power, Tunable Terahertz Radiation from Laser Interaction with a Relativistic Electron Beam

Zhen Zhang,^{*} Lixin Yan, Yingchao Du, Wenhui Huang, and Chuanxiang Tang
Department of Engineering Physics, Tsinghua University, Beijing 100084, China

Zhirong Huang[†]

SLAC National Accelerator Laboratory, Menlo Park, CA 94025, USA

(Dated: September 4, 2018)

We propose a method based on the slice energy spread modulation to generate strong subpicosecond density bunching in high-intensity relativistic electron beams. A laser pulse with periodic intensity envelope is used to modulate the slice energy spread of the electron beam, which can then be converted into density modulation after a dispersive section. It is found that the double-horn slice energy distribution of the electron beam induced by the laser modulation is very effective to increase the density bunching. Since the modulation is performed on a relativistic electron beam, the process does not suffer from strong space charge force or coupling between phase spaces, so that it is straightforward to preserve the beam quality for further applications, such as terahertz (THz) radiation and resonant excitation of plasma wakefield. We show in both theory and simulations that the tunable radiation from the beam can cover the frequency range of 1 ~ 10 THz with high power and narrow-band spectra.

I. INTRODUCTION

High-brightness electron beams have been used to drive free-electron lasers (FELs) [1–3], high-intensity terahertz (THz) radiation [4, 5], advanced accelerators [6–8] and beyond. The precise manipulation of the beam phase-space distribution is often desired to advance the development in the above mentioned fields. Recently, there has been great interest in the generation and control of high frequency structure in the current profile of relativistic electron beams. The bunched beam at picosecond (ps) and sub-ps scale can be used to produce intense narrow-band THz radiation [5, 9] and resonant wakefield excitation [10–13]. Besides, In FELs, sub-ps bunched beams have been applied to generate multicolor X-rays [14] based on the sideband effect [15].

There are several methods proposed and studied for the generation of ps and sub-ps bunching in electron beams, including exchanging transverse modulation to longitudinal distribution [16, 17], direct modulating the drive laser [18–21] and converting wakefield in-

duced energy modulation to density bunching [22–24]. As the development of the state-of-the-art laser technologies, laser-based manipulation of the electron beam has been implemented widely. An external-injected laser pulse which co-propagates with the electron beam inside an undulator can create energy modulation on the scale of the laser wavelength. The energy modulation can be converted into density modulation by letting the beam pass through a longitudinally dispersive element, e.g., a magnetic chicane. However, the typical laser wavelength is usually ~ 800 nm, which is much shorter than the THz wavelength. In this case, the concept of difference frequency can be used to approach THz range with two wavelengths of energy modulation in two separated undulator sections [25–27].

For the laser-based modulation method, since it is performed directly on a relativistic electron beam, the process will not suffer from the strong space charge force or coupling between transverse and longitudinal phase spaces, which is critical to preserve the beam quality for further applications. For example, in resonant wakefield excitation, the transverse focus size of the electron beam needs to match the plasma density [10], which puts a challenging constraint on

^{*} zhen-zhang12@mails.tsinghua.edu.cn

[†] zrh@slac.stanford.edu

the transverse normalized emittance.

In this paper, we propose a method based on the slice energy spread modulation (SESM), rather than energy modulation, to generate sub-ps density bunching in a relativistic electron beam. The slice energy spread of the beam will be modulated in a laser heater [28, 29] if the laser intensity envelop varies periodically. The device has been used widely in the FEL facilities [30–33]. Then after a dispersive section, strong density bunching can be obtained whose wavelength depends on the scale of laser envelope variation, not the laser wavelength. Similar methods have been adopted to generate THz radiation in a storage ring [5] and multicolor X-rays [14]. In this paper, we present detailed theoretical analysis on the conversion from SESM to density bunching and compare it with simulation results. We will also provide an example to produce tunable intense narrow-band THz radiation ranging from 1 to 10 THz. This method is well suited with the configuration of linear accelerator facilities and is of great potential in applications.

This paper is organized as follows. In Sec. II, detailed theoretical analysis on the conversion from SESM to density bunching is presented. It is found that the double-horn slice energy distribution from the laser modulation will help increase the available bunching factor. In Sec. III, we propose a dedicated beam line to generate intense narrow-band THz radiation based on the SESM method. Simulations are performed to demonstrate the tunable bunching frequency. Some discussions about the advantages and requirements of the proposed method will be presented in Sec. IV. Lastly, we will give a short summary in Sec. V.

II. THEORETICAL ANALYSIS

Let us assume the initial beam is uniform in current, but has a Gaussian slice energy spread

$\sigma_\delta(z_0)$ that is a function of the longitudinal coordinate z_0 within the beam. The distribution can be written as

$$f_0(\delta_0, z_0) = \frac{I_0}{\sqrt{2\pi}\sigma_\delta(z_0)} \exp\left[-\frac{\delta_0^2}{2\sigma_\delta(z_0)^2}\right], \quad (1)$$

where δ_0 is the relative energy deviation and I_0 is the beam current. Due to the laser modulation, the slice energy spread is assumed to be

$$\sigma_\delta(z_0) = \bar{\sigma} [1 + A \sin(k_0 z_0)], \quad (2)$$

where $\bar{\sigma}$ is the average rms slice energy spread $0 < A < 1$ is the relative modulation depth. The longitudinal phase space is not uniform but integration over δ_0 yields uniform current I_0 .

An energy chirp is added in the following linac section by $\delta = \delta_0 + h z_0$, and then the longitudinal dispersion occurs in a magnetic chicane as

$$z = z_0 + R_{56}\delta = z_0 + R_{56}(\delta_0 + h z_0). \quad (3)$$

Here we ignore the scale of relative energy spread due to the change of beam average energy, which can be absorbed into other parameters. The density modulation appears after the chicane with the bunching factor as follows

$$b(k) = \frac{1}{I_0} \int d\delta dz e^{-ikz} f(\delta, z). \quad (4)$$

Using the Liouville theorem that $f(\delta, z) = f_0(\delta_0, z_0)$, $d\delta dz = d\delta_0 dz_0$ and making a change of variable from δ_0 to $\eta = \delta_0 / [1 + A \sin(k_0 z_0)]$, we obtain

$$\begin{aligned}
b(k) &= \int d\delta_0 dz_0 e^{-ik(1+hR_{56})z_0 - ikR_{56}\delta_0} \frac{1}{\sqrt{2\pi}\sigma_\delta(z_0)} \exp\left[-\frac{\delta^2}{2\sigma_\delta(z)^2}\right] \\
&= \int d\eta dz_0 e^{-ik(1+hR_{56})z_0 - ikR_{56}\eta[1+A\sin(k_0 z_0)]} \frac{1}{\sqrt{2\pi}\bar{\sigma}} \exp\left[-\frac{\eta^2}{2\bar{\sigma}^2}\right] \\
&= \frac{1}{\sqrt{2\pi}\bar{\sigma}} \int d\eta \exp\left[-ikR_{56}\eta - \frac{\eta^2}{2\bar{\sigma}^2}\right] \int dz_0 e^{-ik(1+hR_{56})z_0} \sum_n J_n(kR_{56}\eta A) e^{-ink_0 z_0}. \quad (5)
\end{aligned}$$

Integration over z_0 yields nonvanishing bunching at the wavenumber $k_n = nk_0/(1+hR_{56})$ with the bunching factor

$$b_n = \frac{(-1)^n}{\sqrt{2\pi}\bar{\sigma}} \int d\eta J_n(k_n R_{56} A \eta) e^{-ik_n R_{56} \eta - \frac{\eta^2}{2\bar{\sigma}^2}}. \quad (6)$$

Numerical calculation of Eq. (6) can be used to find the exact bunching factor and current distribution.

Here we focus only on the fundamental modulation wavenumber $k_1 = k_0/(1+hR_{56})$, the bunching factor b_1 is plotted with a solid line for different $k_1 R_{56} \sigma_0$ in Fig. 1. The expression of b_1 can be simplified if we approximate $J_1(x) \approx a \sin(bx)$ for $|x| < 3$ with $a = 0.58, b = 0.85$, then

$$b_1 = \frac{a}{2} \left[e^{-\frac{k_1^2 R_{56}^2 \bar{\sigma}^2 (1-bA)^2}{2}} - e^{-\frac{k_1^2 R_{56}^2 \bar{\sigma}^2 (1+bA)^2}{2}} \right]. \quad (7)$$

The optimal chicane setting to achieve the largest bunching factor is to satisfy $|k_1 R_{56} \bar{\sigma}| \approx \sqrt{2 + 0.5A^2}$, and the maximum bunching factor is ~ 0.27 .

It should be noted that there is an assumption for the above derivations that the beam has a Gaussian slice energy distribution. This assumption, however, is not always true if we use a laser heater to modulate the beam's slice energy spread. In Ref. [29] it is found that when the laser size is much larger than the electron beam size, the resulting energy profile is a double-horn distribution, which will not contribute much to suppress the instability. Figure 2 shows an example of double-horn distribution of the beam slice energy. The detailed parameter settings can be seen in Table I in the following sections. However, with the purpose to increase the density bunching, we find that the double-horn en-

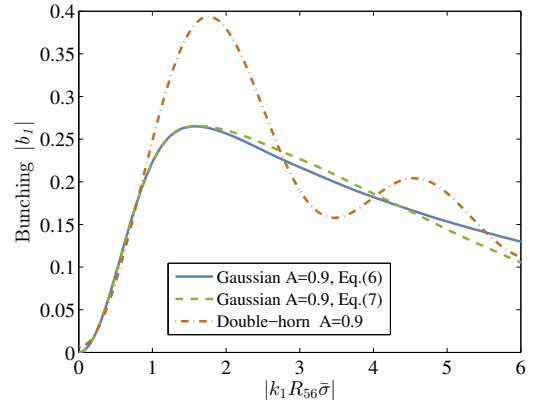


FIG. 1. Bunching factor evolution versus $k_1 R_{56} \bar{\sigma}$ with $A = 0.9$ and different slice energy distributions: (solid line) Gaussian distribution, (dashed line) Gaussian distribution but the bunching factor is calculated by Eq. 7 and (dotted line) double-horn distribution from laser heater.

ergy distribution is more effective to increase the bunching factor in this study.

Assuming the laser spot size is larger than the beam size and the laser power profile has the form $\sqrt{P_L(s)} = \sqrt{\bar{P}}(1 + B \cos(k_0 s))$, the energy modulation in the laser heater can be written as

$$\delta_f = \delta_i + \Delta(1 + B \cos(k_0 s)), \quad (8)$$

with initial and final relative energy deviation δ_i, δ_f and energy modulation amplitude Δ . The full expression for Δ can be found, e.g. in Ref. [29]. To compare with the Gaussian distribution, we define an effective modulation depth

$$\begin{aligned}
A &= \frac{\sqrt{\Delta^2(1+B)^2 + \sigma_0^2} - \sqrt{\Delta^2(1-B)^2 + \sigma_0^2}}{\sqrt{\Delta^2(1+B)^2 + \sigma_0^2} + \sqrt{\Delta^2(1-B)^2 + \sigma_0^2}} \\
&\approx 1 - \frac{2\sqrt{\Delta^2(1-B)^2 + \sigma_0^2}}{\Delta(1+B)}, \quad (9)
\end{aligned}$$

where σ_0 is the initial rms energy spread. When $\Delta/\sigma_0 = 10, B = 1$, the modulation depth

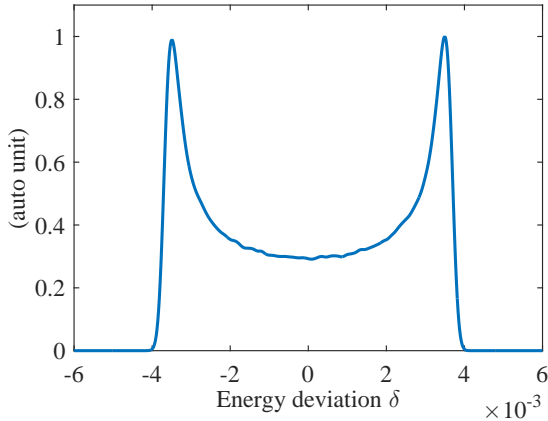


FIG. 2. Double-horn slice energy distribution of the electron beam when the laser spot size is much larger than the beam size in the laser heater. The detailed parameters can be found in Table I.

$A = 0.9$. Numerical calculation results of the bunching factor for different R_{56} are presented in Fig. 1. The optimal R_{56} is similar with the Gaussian case, but the maximum bunching factor is increased to ~ 0.4 with the optimal condition $|k_1 R_{56} \bar{\sigma}| \approx 1.75$.

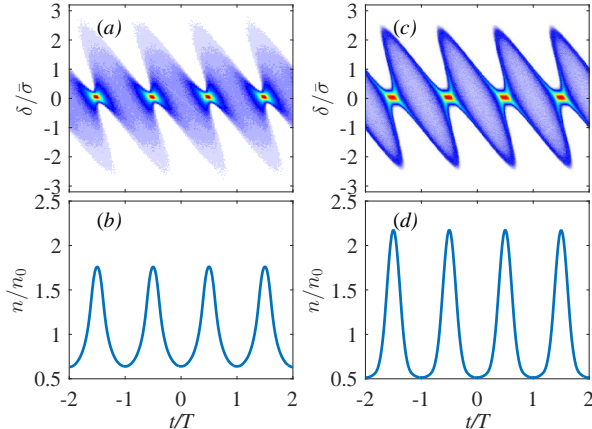


FIG. 3. Longitudinal phase spaces and the corresponding density profile with the largest bunching factor in the two different energy distributions with the same modulation depth $A = 0.9$. The energy is scaled by the rms energy spread and the time is scaled by the period of the bunching. (a) and (b) are Gaussian energy distribution and (c) and (d) are double-horn distribution.

The longitudinal phase spaces and the corresponding density profiles of the electron beam

that give the largest bunching factor in both cases are presented in Fig. 3. The physical meaning of $k_1 R_{56} \bar{\sigma}$ denotes the rotation angle of the phase space. As the increase of the R_{56} , the phase space begins to rotate counter-clockwise and the projected density profile will have peaks and valleys. At a certain angle, the bunching factor reaches its largest value. The similar rotation angle of the two phase spaces in Fig. 3 verifies that they both achieve optimal bunching at similar $k_1 R_{56} \bar{\sigma}$. In order to optimize the bunching for different parts of the beam at the same R_{56} , the modulation depth and the average slice energy spread needs to be uniform over the whole beam. In the double-horn distribution case, the peaks in density profile are higher and sharper, resulting in a larger bunching factor.

III. THZ RADIATION GENERATION

From the theoretical analysis in the previous section, the proposed method using SESM can produce strong density bunching in an relativistic electron beam with a bunching factor about 0.4. Based on this method, we propose a dedicated beam line design for tunable intense narrow-band THz radiation generation in Fig. 4, which can be implemented in most x-ray FEL facilities or dedicated small THz facilities. The electron beam is generated and accelerated by the gun and the first section of linac before it goes into the modulator. In a typical laser heater design, the undulator is located in the center of a chicane to smear out the laser-induced energy modulation. However, we do not have to do this since the density bunching scale of interest here is much larger than the laser wavelength. The drive laser of the gun and the modulation laser can share the same laser system to make the synchronization between electron beam and laser easier. After the modulator, the beam will pass through the second section of linac with $-/+90^\circ$ off-crest acceleration phase to add the energy chirp for THz frequency control without net energy gain. The final chicane is set at optimal value to convert the SESM to density modulation and the radiation frequency is varied by tuning the energy chirp from the second linac. In

practice, the average slice energy spread $\bar{\sigma}$ can be calculated after removing the existing energy chirp.

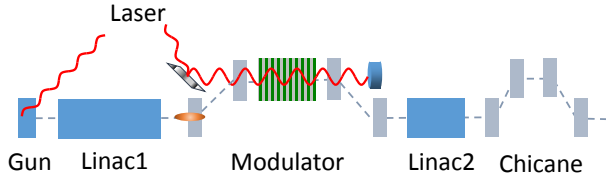


FIG. 4. Schematic layout of the proposed beam line for tunable intense narrow-band THz radiation generation.

The laser pulse with oscillating power envelop can be generated by chirped pulse beating [34] or pulse stacking techniques. In the previous work [5, 14], the laser are both modulated by the first method. Here we discuss the pulse stacking method with α -BBO birefringent crystals [35–37]. Taking 2 THz density modulation as an example, we need to stack laser pulse with a uniform separation 0.5 ps. Using crystals with decreasing thickness and assuming the initial laser pulses is of Gaussian profile with rms width 60 fs, the numerical simulation of the stacked laser pulse train is shown in Fig. 5. For comparison, we also plot the sinusoidal modulation of the same period with full modulation depth (the intensity minimum along the laser pulse is zero).

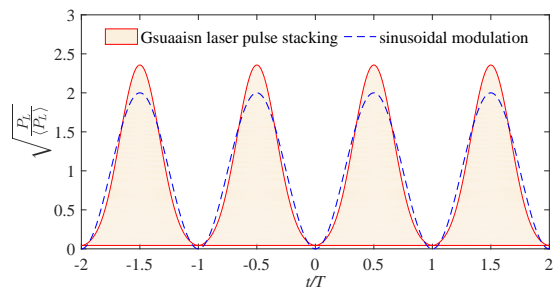


FIG. 5. Laser pulse train distribution. The dashed line denotes the full sinusoidal modulation profile for comparison.

We use the particle tracking code Elegant [38] to simulate the laser modulation and beam dynamics. For similarity, the simulation starts from the end of the first linac with the beam and modulator parameters listed in Table I, which is

realistic and readily available from the injector of many FEL facilities. The current profile of the electron beam is ~ 10 ps flop-top distribution. The laser envelop modulation period is 2 and 4 THz, respectively. Higher frequency modulation can be generated by the chirped pulse beating technique. The waist size of the laser in the modulator is 1.5 mm, much larger than the electron beam size to generate double-horn slice energy distribution as discussed in the previous section.

TABLE I. Beam parameters before the modulator in the simulations.

Parameter	Value	Units
Electron beam		
Charge	500	pC
Beam energy	135	MeV
Current Profile	flat-top	/
Bunch length	~ 10	ps
Intrinsic slice energy spread	10^{-4}	/
Norm. emittance	1	mm-mrad
rms beam size	200	μm
Modulator		
Laser wavelength	800	nm
Undulator period	5	cm
Period number	10	/
Laser waist size	1.5	mm
Laser stacking separation	0.5 (0.25*)	ps
rms laser pulse length	60 (30)	fs
Laser power	1 (0.26)	GW

* The numbers in brackets are the parameters for 4 THz case.

As obtained from the theory, the bunching factor optimizes when $|k_1 R_{56} \bar{\sigma} \approx 1.75|$. For one certain frequency of density bunching, we need to match the R_{56} and the average slice energy spread after the modulator. The energy spread is controlled by the laser power. For the 2 THz case, the laser peak power is 1 GW and the average energy spread after modulator is 190 keV ($1.4e-3$), leading to the optimal $R_{56} = -29.4$ mm. To verify the theoretical prediction, we turn off the Linac2 and scan the R_{56} of the chicane in the simulation. The bunching factor and the peak current are presented in Fig 6. The optimal R_{56} with the largest bunch-

ing factor is -29 mm, which agrees well with the theory. We also present the longitudinal phase space of the beam at the optimal chicane settings in Fig. 7. The residual energy chirp on the beam is due to the linac wakefield and longitudinal space charge effects.

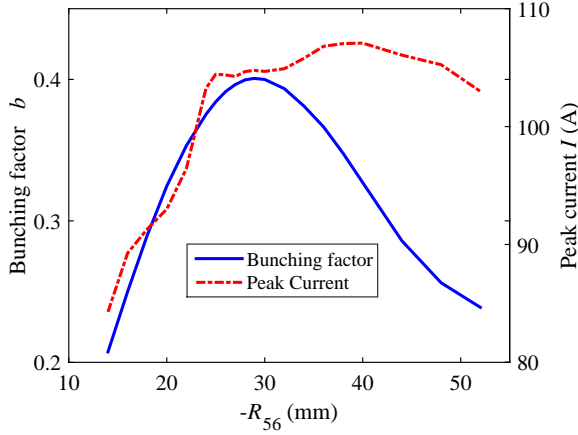


FIG. 6. Bunching factor and peak current of the electron beam with fixed laser power 1 GW and zero energy chirp added onto the beam.

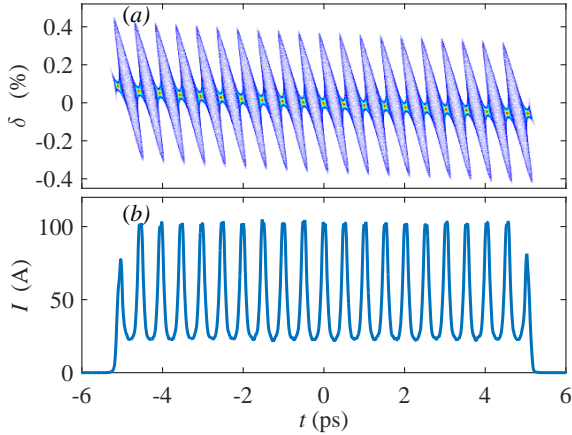


FIG. 7. Phase space of the electron beam with largest bunching factor. $R_{56} = -29$ mm and laser power 1 GW.

The bunching frequency can be controlled by the induced energy chirp from the Linac2 (an S-band acceleration structure in the simulation) before the chicane. As the bunching frequency changes, we need to vary R_{56} and laser power to maintain the bunching factor. If we fix the laser power at 1 GW, the R_{56} needs to be varied

as shown in Fig. 8. The bunching frequency can be varied from 1 to 3 THz with almost constant bunching factor 0.4. We also show the full width of half maximum (FWHM) of the bunching spectra and the requirement for the chirp energy of Linac2. The degradation of the bunching factor and the increase of the spectra bandwidth are both due to the nonlinear effects during the beam compression or stretching.

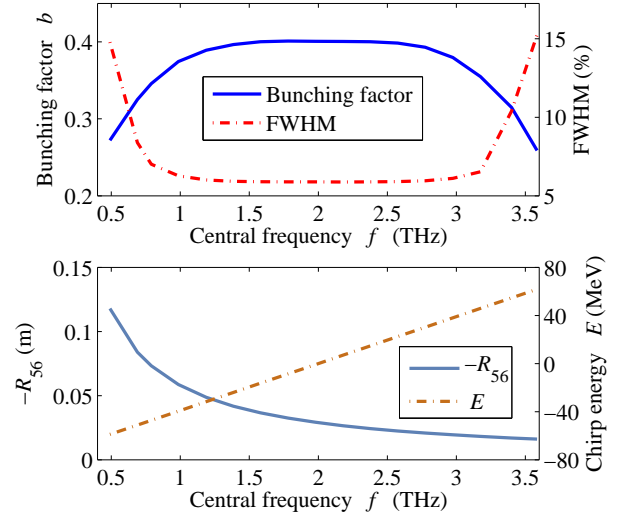


FIG. 8. Bunching factor and the FWHM of the bunching spectra for different radiation frequency by matching the R_{56} and chirp energy. The laser power is fixed at 1 GW.

In addition, we can also choose to vary the laser power and fix the R_{56} . Figure 9 presents the results of bunching factor, FWHM, required laser and chirp energy for different frequencies, which are similar with the results of varying R_{56} . In practice, we can vary both R_{56} and laser power to optimize the bunching factor for different frequencies based on the availability of the beam line.

Lastly, we present some examples of 4 THz density modulation simulations. As the frequency is increased by a factor of 2, the laser power is decreased to 0.26 GW to meet the optimal condition with $R_{56} = -29$ mm. By varying R_{56} , the bunching frequency can be varied between 2 to 6 THz with a bunching factor larger than 0.3, as shown in Fig. 10. However, if we add a harmonic RF cavity that decelerates the

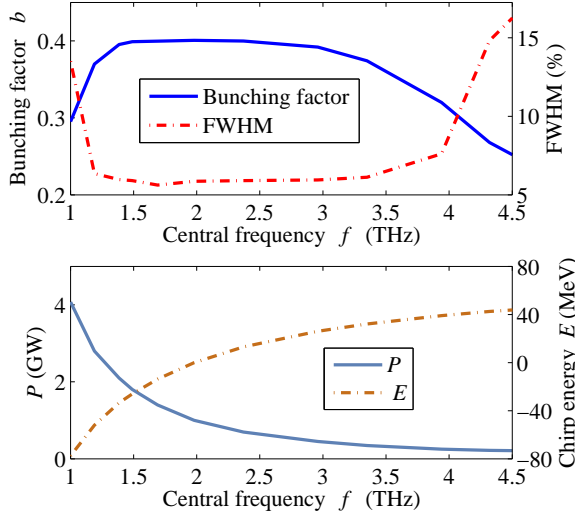


FIG. 9. Bunching factor and the FWHM of the bunching spectra for different radiation frequency by matching the laser power and chirm energy. The R_{56} is fixed at -29 mm.

beam at -180° before the chicane to compensate for the nonlinear effects during compression, the frequency range of the modulation can be extended significantly. In Fig. 10, we give the requirements for R_{56} , chirm energy, and especially the maximum energy gain of a 4th-harmonic (X-band) cavity to vary bunching frequency. With the help of chirm compensation from the X-band cavity (e.g. [39]), the bunching frequency range is extended from 1 to ~ 8 THz with the bunching factor keeping at ~ 0.38 .

Note that the bunching frequency control discussed above is to compress or stretch the electron beam. Alternatively we can also change the laser intensity modulation period directly to control the bunching frequency. As the increase of bunching frequency k_1 , the R_{56} of the chicane or (and) the laser power needs to be decreased to keep the optimal condition. Usually laser-induced energy spread should be much larger than the initial slice energy spread to introduce enough effective modulation depth, so reducing the R_{56} of the chicane will be a better choice. Compared with the beam compression, in this method the nonlinear effects in the chicane will be smaller, which is helpful to maintain the density bunching. In addition, the number of sub-bunches in the train will become larger for higher

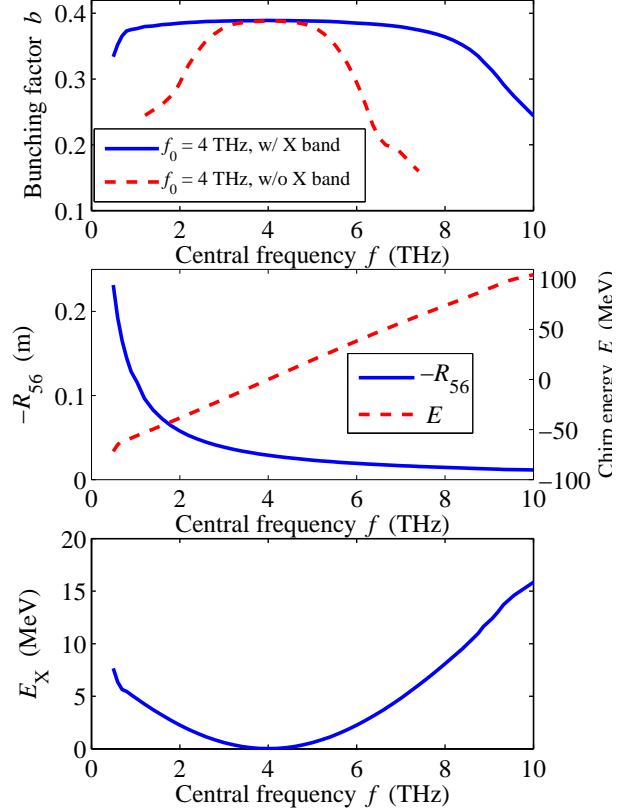


FIG. 10. (top) Bunching factor for different radiation frequency w/ and w/o X-band cavity. (middle) The requirements for R_{56} and chirm energy. (bottom) The requirement for energy gain of X-band cavity.

modulation frequency, resulting in smaller bandwidth in the spectra.

IV. DISCUSSIONS

The proposed method is of great advantages in the generations of tunable narrow-band THz radiation. The bunching factor averaged over the beam can be kept around 0.4 for a wide range of frequency, covering the THz gap, by varying the beam compression and (or) the laser modulation period. The proposed method is robust as it is performed on a very relativistic electron beam. Since there is no strong space charge force or beam loss during the process, the beam quality can be preserved for beam matching and focusing. Assuming that the beam is focused to a small spot and the frequency cut due to finite dimensions of the target, e.g., a metallic foil, can

be neglected, it is possible to estimate the THz energy emitted by this beam as

$$E_{\text{THz}} = N_e^2 b^2 \frac{dW_1}{d\omega} \Delta\omega, \quad (10)$$

where b is the bunching factor, N_e is the number of electrons for coherent emission, $\frac{dW_1}{d\omega}$ is the single particle spectral power which for transition radiation is relative relatively flat and equal to $\frac{2}{\pi} m_e r_e c \ln \gamma$, with m_e the rest electron mass and r_e the classical electron radius. $\Delta\omega$ is the linewidth which is equal to 1 over the number of cycles in the pulse train. In the previous simulations, the beam charge is set at 0.5 nC. Even though there is no strict constraint on beam charge and beam repetition rate. Using 2 THz radiation as an example, the THz pulse energy emitted from 10-ps beam is shown in Fig. 11 as a function of beam charge. When the charge is 2 nC, the pulse energy is up to more than $40 \mu\text{J}$ centered around 2 THz frequency in 5% bandwidth. The spectra brightness and THz field are both significantly improved. Finally, we note that using an undulator [9] or a dielectric tube [24, 40, 41] can further enhance the output THz energy to approach the mJ level.

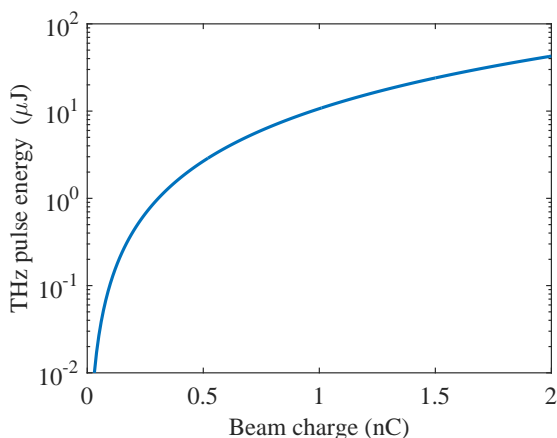


FIG. 11. THz pulse energy around 2 THz frequency in 5% bandwidth emitted from 10-ps beam for different beam charge.

In passing we note that our proposal does not require a linac with a photo-cathode RF gun. The method is also applicable for the electron beams from storage rings or thermal-cathode injectors with higher repetition rate. The main requirement of the method is the electron beam energy needs to be $\sim 100 \text{ MeV}$ to be resonant with an optical laser. However, for electron beams with lower energies, it is still possible to interact harmonically with the optical laser.

V. SUMMARY

In this paper, we have proposed a method based on the slice energy spread modulation to generate strong density bunching in a relativistic electron beam, which can be used to produce intense narrow-band THz radiation. Theoretical analysis and simulations both show that with the help of double-horn slice energy spread distribution from the laser modulation, the bunching factor can reach up to 0.4 for modulation frequencies ranging from 1 to 10 THz. We also found the optimal condition involving the bunching frequency, R_{56} of the conversion section and the average slice energy spread to maximum the bunching factor. To implement this scheme in an existing x-ray FEL, very minimal hardware additions are required. The use of the laser in our proposal makes the THz signal synchronize with the optical signal and has a stable waveform. The high spectra brightness of the radiation make it a powerful and promising method for many applications, such as THz pump [42], THz streaking [43] and THz acceleration [44].

VI. ACKNOWLEDGE

We thank Enrico Allaria and Agostino Marinelli for very helpful discussions. This work was supported by the National Natural Science Foundation of China (NSFC Grants No. 11375097, No. 11435015 and No. 11475097) and U.S. Department of Energy Contracts No. DE-AC02-76SF00515.

-
- [1] W. Ackermann *et al.*, Nat. Photonics 1, 336 (2007).
- [2] P. Emma *et al.*, Nat. Photonics 4, 641 (2010).
- [3] T. Ishikawa *et al.*, Nat. Photonics 6, 540 (2012).
- [4] G. L. Carr *et al.*, Nature 420(6912), 153-156 (2002).
- [5] S. Bielawski *et al.* Nature Physics, 4(5), 390-393 (2008).
- [6] I. Blumenfeld *et al.* Nature, 445(7129), 741-744 (2007).
- [7] M. Litos *et al.* Nature, 515(7525), 92-95 (2014).
- [8] C. Jing *et al.*, Phys. Rev. Lett. 98, 144801 (2007).
- [9] A. Gover, Phys. Rev. ST Accel. Beams 8, 030701 (2005).
- [10] P. Chen, J. M. Dawson, R. W. Huff and T. Katsouleas, Phys. Rev. Lett. 54(7), 693 (1985).
- [11] R. D. Ruth, P. L. Morton, P. B. Wilson and A. W. Chao, Part. Accel., 17, 171 (1984) and SLAC-PUB-3374.
- [12] P. Schutt, T. Weiland and V. M. Tsakanov, in *Proceedings of the Second All-Union Conference on New Methods of Charged Particle Acceleration* (Springer, New York, 1989).
- [13] J. G. Power, W. Gai, X. Sun and A. Kanareykin, In Particle Accelerator Conference, 2001. PAC 2001. Proceedings of the 2001 (Vol. 1, pp. 114-116). IEEE.
- [14] E. Roussel *et al.* Phys. Rev. Lett. 115, 214801(2015).
- [15] Z. Zhang *et al.* Phys. Rev. Accel. Beams 19, 050701 (2016).
- [16] P. Muggli *et al.*, Phys. Rev. Lett. 101, 054801 (2008).
- [17] Y. E. Sun *et al.*, Phys. Rev. Lett. 105, 234801 (2010).
- [18] Y. Shen *et al.*, Phys. Rev. Lett. 107, 204801 (2011).
- [19] Y. Li and K. J. Kim Appl. Phys. Lett. 92, 014101 (2008).
- [20] P. Musumeci, R.K. Li, and A. Marinelli, Phys. Rev. Lett. 106, 184801 (2011).
- [21] Z. Zhang *et al.*, Phys. Rev. Lett. 116, 184801 (2016).
- [22] S. Antipov *et al.*, Phys. Rev. Lett. 108, 144801 (2012).
- [23] K. Bane and G. Stupakov, Nucl. Instrum. Methods Phys. Res., Sect. A 677, 67 (2012).
- [24] S. Antipov *et al.*, Phys. Rev. Lett. 111, 134802 (2013).
- [25] D. Xiang and G. Stupakov, Phys. Rev. ST Accel. Beams 12, 080701 (2009).
- [26] M. Dunning *et al.*, Phys. Rev. Lett. 109, 074801 (2012).
- [27] Z. Wang, D. Huang, Q. Gu, Z. Zhao and D. Xiang, Phys. Rev. ST Accel. Beams 17, 090701 (2014).
- [28] E. L. Saldin, E. A. Schneidmiller and M.V. Yurkov, Nucl. Instrum. Methods Phys. Res., Sect. A 528, 355 (2004).
- [29] Z. Huang *et al.* Phys. Rev. ST Accel. Beams 7, 074401 (2004).
- [30] Z. Huang *et al.* Phys. Rev. ST Accel. Beams 13, 020703 (2010).
- [31] E. Ferrari *et al.* Phys. Rev. Lett. 112, 114802 (2014).
- [32] S. Spampinati *et al.* Phys. Rev. ST Accel. Beams 17, 120705 (2014).
- [33] J. Lee *et al.* Nucl. Instrum. Methods Phys. Res., Sect. A 843, 39 (2017).
- [34] A. S. Weling and D. H. Auston, J. Opt. Soc. Am. B 13, 2783 (1996).
- [35] J. Power and C. Jing, AIP Conf. Proc. 1086, 689 (2009)
- [36] P. Musumeci, J. T. Moody, C. M. Scoby, M. S. Gutierrez, M. Westfall, and R. K. Li, J. Appl. Phys. 108, 114513 (2010).
- [37] L. X. Yan *et al.* J. Plasma Phys. 78, 429 (2012).
- [38] M. Borland, ELEGANT, Advanced Photon Source LS-287, 2000.
- [39] P. Emma, X-Band RF Harmonic Compensation for Linear Bunch Compression in the LCLS, SLAC-TN-05-004 (2001).
- [40] A. M. Cook *et al.* Phys. Rev. Lett. 103, 095003 (2009).
- [41] G. Andonian, *et al.* Appl. Phys. Lett. 98, 202901 (2011).
- [42] M. Liu *et al.* Nature 487, 345348 (2012).
- [43] U. Frühling *et al.* Nature Photonics 3, 523-528 (2009).
- [44] E. A. Nanni *et al.* Nature Communications 6, 8486 (2015).